CHALMERS

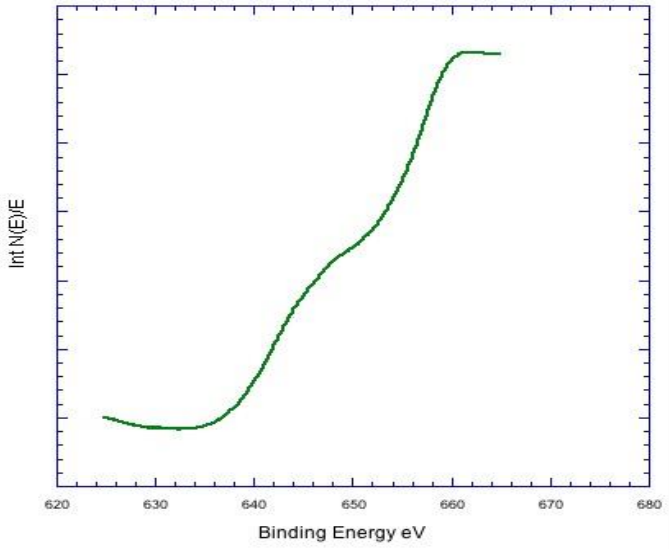

Determining the concentration of manganese in (Ga,Mn)As by means of X-ray Photoelectron Spectroscopy

Master thesis in the Master Degree Programme, Applied Physics

ORHE ARUVIERE

Department of Applied physics
CHALMERS UNIVERSITY OF TECHNOLOGY
Goteborg, Sweden, 2014.

Determining the concentration of manganese in (Ga,Mn)As by means of X-ray Photoelectron Spectroscopy

ORHE ARUVIERE

CHALMERS

Department of Applied physics
CHALMERS UNIVERSITY OF TECHNOLOGY
Göteborg, Sweden, 2014.

Determining the concentration of manganese in (Ga,Mn)As by means of X-ray photoelectron spectroscopy

ORHE ARUVIERE

Department of Applied Physics

Chalmers University of Technology

SE-41296 Gothenburg

Sweden

Telephone +46 (0)31-7721000

Göteborg, Sweden 2014

ABSTRACT

This thesis work investigates the ability of x-ray photoelectron spectroscopy(XPS) to assess the Mn concentration in the $Ga_{1-x}Mn_xAs$. For this purpose measurements were the performed on samples with different nominal Mn concentrations in the range 0.5-5%. The samples were sputtered with argon ions to remove surface oxide and carbon contamination, and to record the depth distribution of Mn.

The results show that the method can be used for the estimation of the Mn concentration provided that the (XPS) sensitivity factors used are accurate, a correct background is used and that the spectra are recorded with good statistics.

Keywords: (Ga,Mn)As, Mn concentration, x-ray photoelectron spectroscopy, sensitivity factor, molecular beam epitaxy.

ACKNOWLEGEMENT

First of all I would like to give thank the almighty God for the protection and love he have show me throughout my entry life without you I would not be here today. I want to use this opportunity to give thanks to my project supervisor professor Janusz Kanski for his patient, care and contribution for the success of the project work because without your help the work will not be complete today. I would also want to thank Lars llver for the help in collection of the data from the XPS machine and explanation of how the XPS machine work.

Secondly I want to thank my dad and mom Mr. Raphael Orhe and Mrs. Mary Orhe for the encouragement and advise you give me to strive to be successful in life and to be a better person. To my brothers and sister omo-efe, Akpobaro, Okierumute, Ovieraya and Enajite. I want to say that I appreciated the love you all show me and I am very happy to be your brother and sister. To my late brother Ogheneochuko, I want to dedicate the project work to you and I will never stop thinking about you, we all miss you.

Thirdly I want to say thank to my wife Mrs. Marie Orhe, my daughter Elisha and my son Noah for the support, love and care they have given me and my father in-law Stig Eriksson and his family for welcoming me into their family.

Lastly, I would like to thank my friends whom I meet in Sweden Daniel, Samuel for accommodating me when I needed a place to stay in Goteborg, Gibson, Abiodun, Gani, Joseph and Christopher. And for those friends i did not mention there name here, I want to say i appreciate the contribution you have made in my life thank you all.

TABLE OF CONTENTS

Chapter 1

Introduction

In the field of information technology the concept of spintronics is considered as a path to continued development of processing capabilities. An approach in this direction is to integrate data processing and storing by using magnetic semiconductor materials. In the course of the years' research, (Ga,Mn)As has become one of the most promising materials for this purpose because of its magnetic properties and compatibility with the existing III-V heterostructure technology. Studies of diluted magnetic semiconductor, centered mostly on IV-VI or II-VI semiconductors, have been known for some time. The disadvantage of these materials is that they are difficult to dope to create p- and n- type, which makes them less attractive for application. Furthermore, they exhibit very low Curie temperatures (T_C) and they are difficult to manufacture. The successful growth of (In,Mn)As films on GaAs substrates 1989 [1], where carrier induced ferromagnetism was found [2], and also of (Ga,Mn)As in 1996 [3], eliminated these shortcomings.

Molecular beam epitaxy can be used to produce (Ga,Mn)As by introducing Mn (up to 20%) to GaAs. In addition to introducing magnetic moments, Mn atoms in Ga substitutional sites act as acceptors and provide holes that mediate ferromagnetic interaction between the local moments of the open d shells in the Mn atoms. T_C increases with increase in Mn concentration and hole concentration [4,5] in the range of 160-173K [6,7] . The increase in the Mn concentration can only be obtained at a cost of increased density of defects. The most important of these are now known to be As antisites and Mn interstitials that act as double donors. The latter can be removed by post growth annealing below 250℃ [8,9]. Among the practical problems with ternary systems like (Ga,Mn)As is the determination of element concentrations. The focus of this thesis work is on the assessment of the concentration of manganese in (Ga,Mn)As using X-ray photoelectron spectroscopy (XPS).

This report is divided into six parts: chapter 2 gives a description of the structure of (Ga,Mn)As and its properties. Chapter 3 covers the molecular beam epitaxy, the growth of (Ga,Mn)As and principle of X-ray photoelectron spectroscopy. Chapters 4 and 5 are devoted to the experimental work, results and discussion and chapter 6 gives a conclusion of this work.

Chapter 2

Structure and Properties of (GaMn)As

2.1 Crystallographic structure

The crystal structure of GaAs is zinc blende, which can be described as a combination of two face centered cubic lattices. One sublattice contains the anions and the other contains the cations. They are displaced ¼ of a cube diagonal relative each other. In the tetrahedral arrangement each gallium atom is attached to four As atoms and vice versa. There are four molecules of GaAs per unit cell with a lattice constant (a_0) equal to 5.65 Å. This parameter has been studied experimentally [10] and theoretically [11]. It has been shown that the lattice constant of (Ga,Mn)As depends on the concentration of both the As antisite and Mn interstitial defects. At very low Mn concentrations, the (Ga,Mn)As lattice constant slightly decreases with increasing Mn content, up to the Mn content at which the As antisite donors are fully compensated by the Mn acceptors. Further increasing of Mn concentration leads to an increase of the lattice constant due to the manganese at the gallium sites and the increased density of the manganese at interstitial sites [10] .

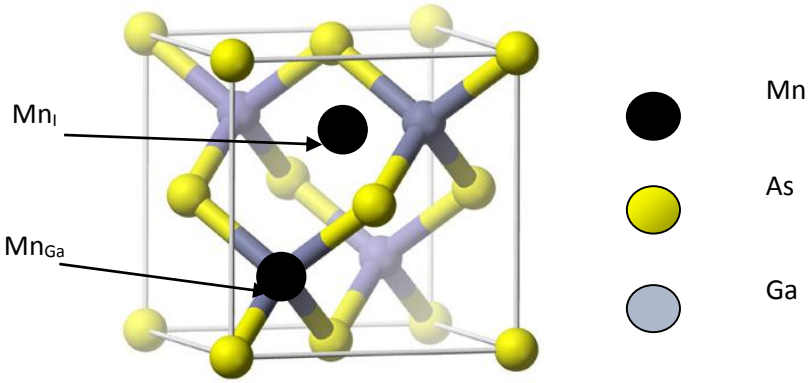

Figure 2.1: Schematic diagram of the unit cell of the zinc blende structure and the positions of Mn_{Ga} binding to four As atoms.

2.2 Magnetic and Transport properties

The magnetic properties of (Ga,Mn)As originate from the magnetic moment introduced by the Mn ions that can be incorporated both in Ga substitutional and interstitial positions. The magnetic and transport properties were studied [12] for series of (Ga,Mn)As thin films grown under various conditions. At relatively high ($x>0.05$) or low ($x<0.03$) Mn concentration, (Ga,Mn)As showed respectively metallic or semiconducting behavior, which was found to be

insensitive to the growth condition [13]. Fig 2.2 shows a diagram of the properties of (Ga,Mn)As in relation to the two main growth parameters, growth temperature and Mn concentration x. (Ga,Mn)As grown at lower temperature, below ~200°C, is paramagnetic and semiconducting, whereas (Ga,Mn)As grown at higher temperature, above ~250, is ferromagnetic and metallic.

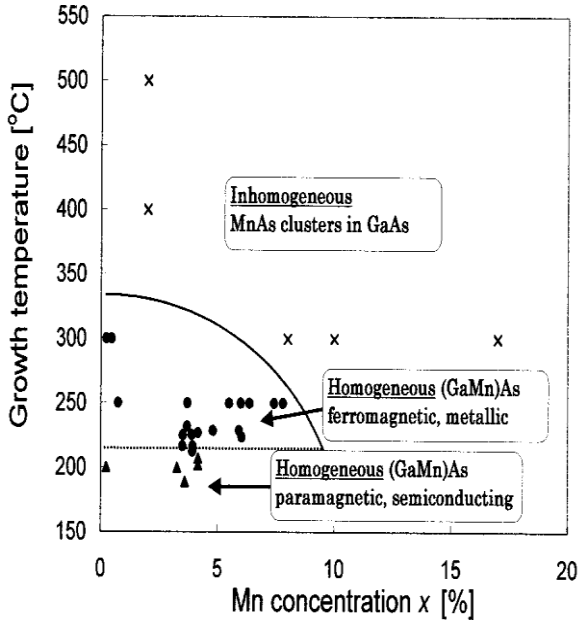

Figure 2.2: The diagram shows the properties of (Ga,Mn)As in relation to two growth parameters, the growth temperature and Mn concentration x.Transport and magnetic properties of the homogeneous (GaMn)As shown to depend on the growth temperature [13].

Magnetic anisotropy describes the tendency of a material to magnetize in a certain direction. An easy axis is the favorable direction of magnetization that is determined by the source of magnetic anisotropy. Some sources of magnetic anisotropy are magnetocrystalline anisotropy, shape anisotropy and magnetoelastic anisotropy. The magnetic anisotropy of (Ga,Mn)As has been found to depend on many parameters such as temperature, strain and carrier density [14]. (Ga,Mn)As epilayers have a strong in-plane unidirectional anisotropy component [14,15,16]. The easy axis is in –plane for compressive strain and out- of -plane for tensile strain [16]. The ability to manipulate the easy axis orientation from in-plane to out-of-plane has many advantages for fundamental research on DMS materials e.g spintronic, where electron spin is used to carry information and is very important for application in the magnetic recording technologies [17].

2.3 Optical properties

(Ga,Mn)As has been studied using modulation photoreflectance spectroscopy and Raman spectroscopy with Mn content up to 1.2% [18]. The results revealed a decrease in the band-gap-transition energy with increase in Mn content in very low doped (Ga,Mn)As layers with n-type

conductivity. This was interpreted as a result of merging the Mn- related impurity band with the host GaAs valence band [18] . On the other hand, increase in the band-gap-transition energy with increased Mn content in the (Ga,Mn)As layers with p-type conductivity indicated the Moss-Burstein shift of the absorption edge due to the Fermi level located within the valence band, determined by the free-hole concentration[18].

2.4 Electronic properties

The conduction band, valence band and doping play a very important role for understanding electronic properties of all semicondutors, including (Ga,Mn)As. Figure 2.3 shows the band structure of GaAs at 300K. The degeneracy of the valence bands at the centre of the Brillouin zone is partially lifted by spin-orbit coupling into a doubly degenerate valence band (heavy and light holes) and a split-off band. The spin split-off band is 0.34 eV below the valence band maximum. Mn ($4s^2 3d^5$) substitutes for the valence Ga^{3+}. From electron-spin resonance (ESR) measurements, it was shown that the Mn^{2+} configuration in GaAs is ($3d^5$ + hole) or $3d^4$ [19].

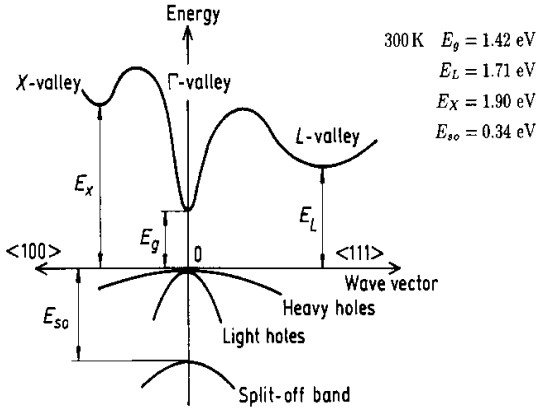

Figure 2.3: The band structure of GaAs near the valence band maximum [20].

Chapter 3

Experimental methods

3.1 Molecular beam epitaxy

Molecular beam epitaxy (MBE) is a technique for epitaxial growth of material via the interaction of one or several molecular or atomic beams that occurs on the surface of a heated crystalline substrate under ultra-high vacuum (UHV). The term epitaxy is derived from the Greek words epi (meaning "on") and taxis (meaning "arrangement") .Thus epitaxy can simply be described as 'surface arrangement'. The MBE technique is used in the production of high quality epitaxial structure with monolayer control. The ultra-high vacuum ensures a clean, dust free environment of surface and growing epitaxial film. With the evolution of MBE, material can be grown on insulators, oxides, metal, superconductors as well as semiconductor material such as silicon, germanium or gallium arsenide.

Homoepitaxy refers to the case where deposited material is the same as the substrate, but if material deposited is different from the substrate then the term heteroepitaxy is used. The process and application of MBE has been in practice for long, the works of Arthur [21] and Cho [22] brought a significant understanding of how the process is applied to compound semiconductor growth. MBE has been found useful in the manufacture of semiconductor devices such as grouped below:

1. **Transistors**: Inverted HEMT [23], low noise HEMT [24], Strained-layer [25], BIFET (Buried-Interface FET) [26], BICFET (Bipolar Inversion Channel FET) [27], and TEBT (Tunneling Emitter BT) [28].
2. **Microwave Devices**: IMPATT [29]-[31], MIXER [32]-[34], GUNN [35], VARACTOR [36][33]
3. **Optoelectronic Devices**: These include photodetectors such as solar cell [37], SEED (Self Electro-optic Effect Devices) [38], GeSi Waveguide [39].
4. **Integrated Devices/Circuits**: These can be sub divided into
   - **a-** Analog ICs: 115 GHz Oscillator [40], HBT Voltage Comparator [41]
   - **b-** Digital ICs: 1Kb SRAM [42], 4Kb SRAM[43], Quantum-Well CCD[44], HBT ICs [45]
   - **c-** OEICs: LED/Amplifiers [46], Photoreceiver [47]-[49], Transmitter/receiver [50], Laser/FET [51]
   - **d-** Optical ICs [52]: Optical Switch [53], Laser Taper Coupler [54], Laser/Waveguide [55]

The principle of MBE is based on shooting molecular beams from effusion cells (containing different materials such as Al, As and Si depending on the crystal to create) on the surface of the heated substrate. The atomic or molecular beams impinge on a hot substrate causing the crystals to build up very slowly and systematically in atomic layers. An illustration of this is shown on figure 3.1.

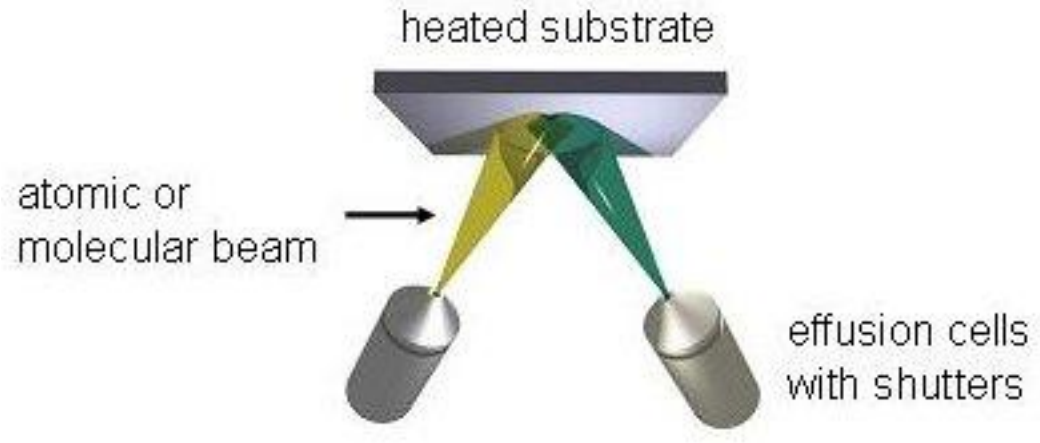

Figure 3.1: Basic principle of molecular beam epitaxy showing coevaporation of atoms or molecules from two different sources onto a heated substrate (C. Kreis, Ph.D. thesis).

There are other types of epitaxial growth techniques which include liquid-phase epitaxy (LPE), metalorganic vapor-phase epitaxy (MOVPE), metalorganic vapor-phase deposition (MOCVD) and hydride vapor-phase epitaxy (HVPE). The choice of MBE vs other growth techniques depends on the desired structure and needs. In the case of mass production, for example, MBE suffers from a lower yield compared to LPE and MOCVD due to a lower growth rate and wafer capability (currently, GaAs- based MBE production systems are capable of up to 4X6" diameter wafers, compared to 5X10" of MOCVD) [56]. When requirements such as abruptness and control of interfaces and doping profiles are critical, MBE is the proper technique to use due to its lower growth temperature and growth rate [56]. MBE is farthest from the thermal equilibrium and is therefore best suited for the preparation of a metastable system like (Ga,Mn)As.

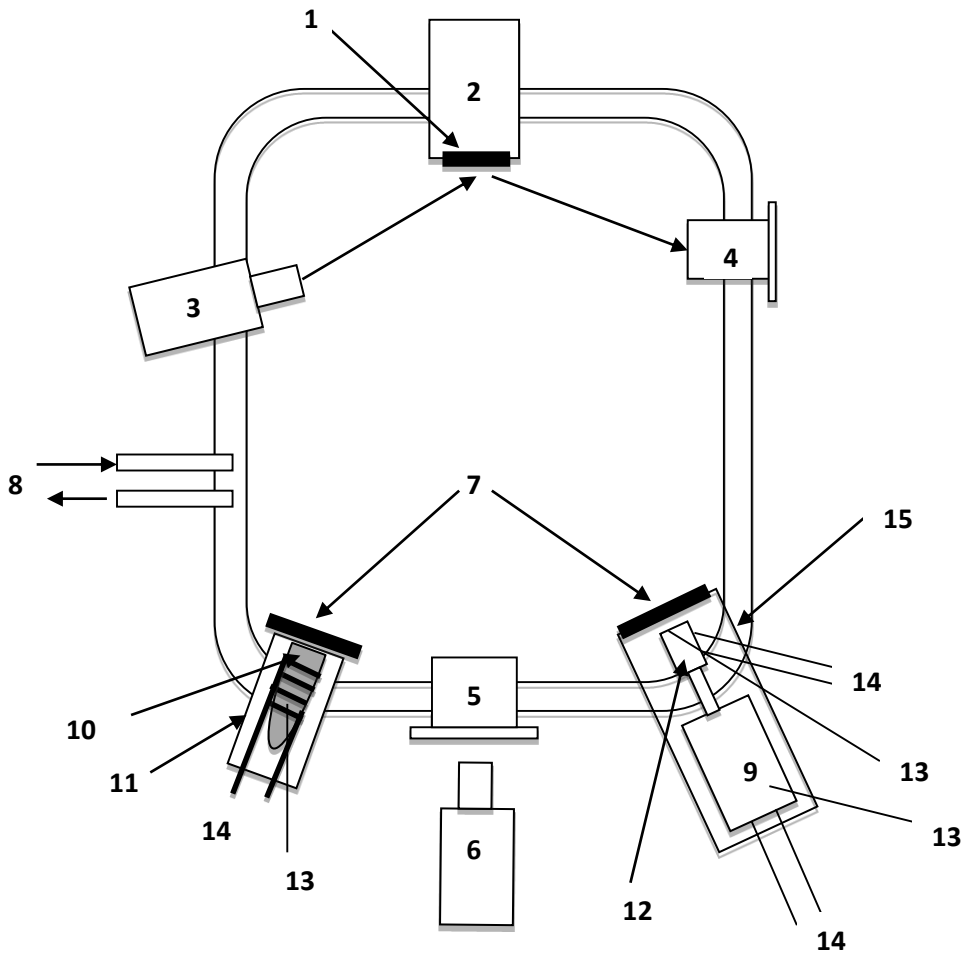

1. Substrate
2. Manipulator including a substrate heater
3. RHEED gun
4. Viewport with fluorescent RHEED screen
5. Heated viewport
6. Infrared pyrometer
7. Beam shutter
8. Liquid N_2 for cooling of cryopanel
9. As tank
10. PBN crucible
11. Effusion cell: Ga, ln and Bi
12. As cracker
13. Thermocouple(connected to a thermal regulator)
14. Wire for resistive heater (connected to a thermal regulator)
15. Effusion cell: As valved cracker source

Figure 3.2: A schematic picture of the MBE system

3.2 Growth of (Ga,Mn)As

(Ga,Mn)As is grown with MBE on GaAs substrates when the substrates temperature during the growth process is below 250℃ [8,9], which is much below the growth temperature of GaAs 590-640℃ [57]. For (Ga,Mn)As much lower temperature must be used to prevent segregation of MnAs (MnAs is a ferromagnetic metal with ferromagnetic to paramagnetic phase transition temperature of 40 ℃). To minimize the As antisites defects, maximum growth temperature, slightly below MnAs segregation threshold, [57] is used.

3.3 Post-growth annealing

Post–growth annealing is the process of removing Mn_I (Mn interstitials) defects from (Ga,Mn)As bulk. During annealing the weakly bound Mn interstitials diffuse and those reaching the surface are passivated either by oxidation or nitridation, when the (Ga,Mn)As layer is exposed in air or in N_2. The drawback of this method is that no further growth can be made on this surface. An alternative method is by capping the grown (Ga,Mn)As with amorphous As and bind the diffusing Mn to the As. The excess As can then be desorbed by further short heat treatment up to 250 ℃ [8,9] see fig3.3. One advantage of the latter method is that a much shorter annealing time is needed, ~2h, compared to ~200 for annealing in air. The sample surface is still clean and atomically flat with no oxidation. The most important advantage of the method is that further layer can be grown on the surface.

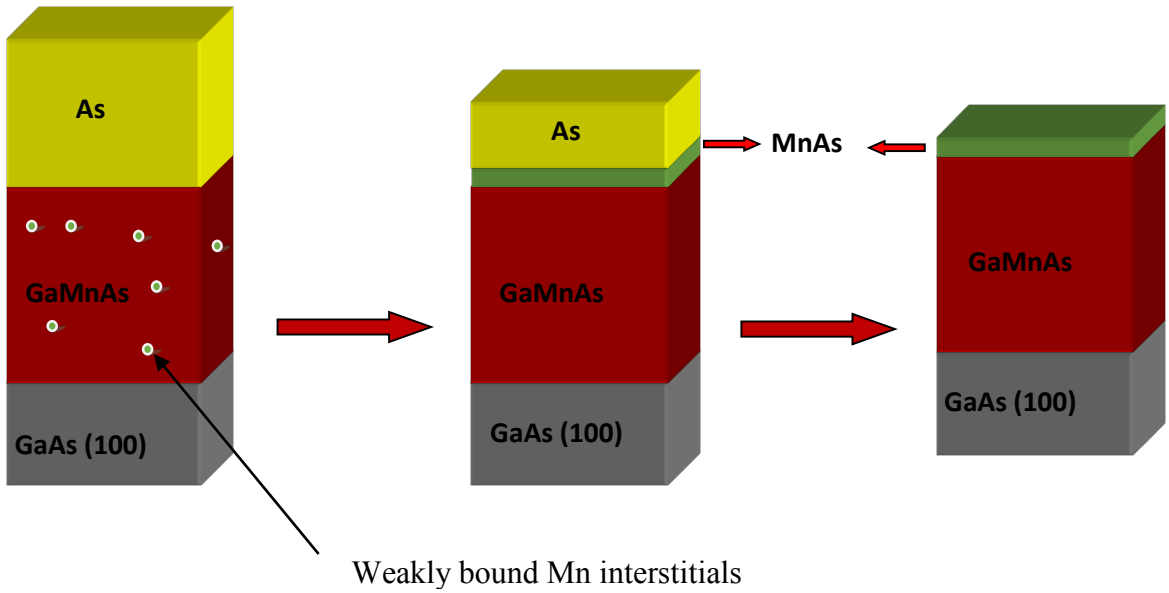

Fig 3.3: Schematic diagram of removing Mn interstitials from (Ga,Mn)As by post-growth annealing with coated amorphous arsenic layer.

3.4 Reflection High Energy Electron Diffraction (RHEED)

RHEED, a technique of monitoring sample surface during growth, is a very sensitive and diagnostic tool for observing changes in the structure of the surface layers as a function of the growth parameters. It is possible to obtain information on surface structure and the smoothness from RHEED patterns. An electron gun and a fluorescent screen are the two key components of a RHEED setup. See figure 3.4

The electron gun generates a high energy (up to 20 keV) collimated beam of monoenergetic electrons. The beam is incident on the sample surface at a glancing angle of 1-4°, which makes the method surface sensitive in spite of the high energy. The diffracted pattern of electrons is observed on a fluorescent screen.

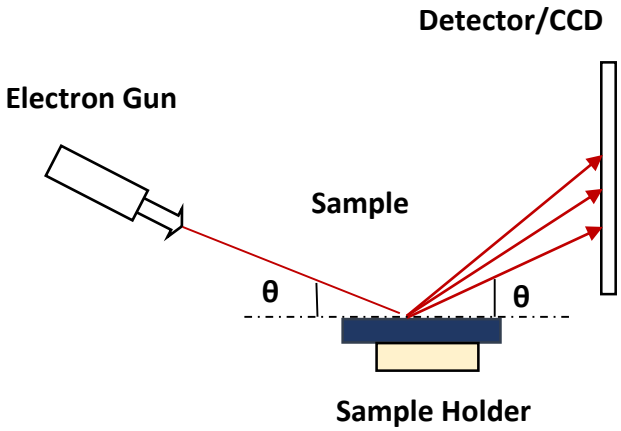

Figure 3.4: Schematic RHEED setup

3.5 RHEED Oscillations

RHEED oscillations can be used for monitoring the formation of individual atomic layers during MBE growth. The principle involves variation of the electron scattering which can be monitored by observing a RHEED spot intensity (e.g. the specular beam). The RHEED intensity oscillations contain morphologic information of the growth kinetics. The degree of roughness corresponds to each fraction of a ML growth with a maximum roughness and hence low intensity for 0.5MLdeposited and a maximum smoothness and hence high intensity for the surface after each full ML [58]. This is shown diagrammatically in figure 3.5. The concentration of Mn is given by $x=\Delta f/f$, where f is the oscillation frequency during growth of (Ga,Mn)As and Δf is the difference between the oscillation frequencies during growth of (Ga,Mn)As and LT-GaAs. There are two problems with this method to determine the Mn concentration.

First, it only measures Mn in substitutional lattice positions and second, the oscillations are not always sufficiently clear. Therefore an alternative method is needed as a complement.

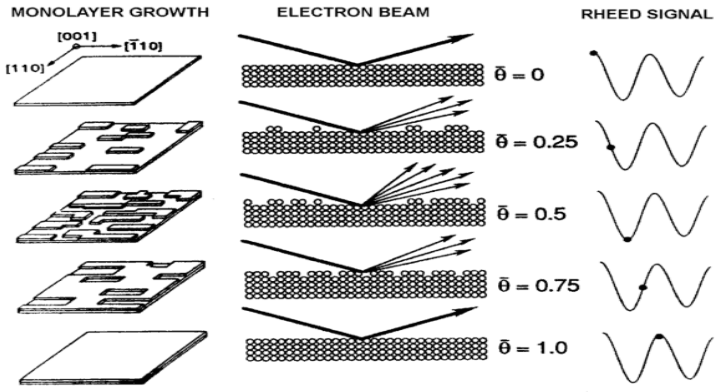

Figure 3.5: Mechanisms of RHEED intensity oscillations during growth of a monolayer [58].

3.6 X-ray photoelectron spectroscopy (XPS)

XPS, also known as electron spectroscopy for chemical analysis (ESCA) is an analytical technique for investigating the elemental and chemical composition of solid surfaces. XPS, was developed in the mid 1960's by Kai Siegbahn [59] and makes use of photoelectric effect. This principle involves monoenergetic soft X-rays irradiating a sample and exciting core electrons. The number of electrons that escape from its surface is measured as function of their kinetic energy, see fig 3.6. The most common laboratory X-ray sources are MgKα (1253.6 eV) and AIKα (1486.6 eV). The basic physics of this process is described by the Einstein equation [60]

$$KE = hv - BE - \emptyset_s \quad \text{.....(1)}$$

where KE is the kinetic energy, hv is the energy of the photons, BE is the binding energy of the atomic orbital from which the electron originates, and φ_s is the spectrometer work function.

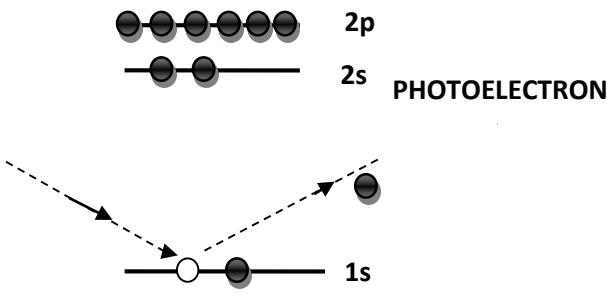

Figure 3.6: Diagram of the photoelectric process.

The probability of an electron to travel a distance, d, through a material without undergoing inelastic scattering is

$$P(d) = e^{(-d/\lambda)} \quad \ldots\ldots\ldots\ldots\ldots\ldots\ldots\ldots\ldots\ldots\ldots\ldots\ldots\ldots\ldots\ldots\ldots\ldots\ldots (2)$$

where λ is the inelastic mean free path (IMFP), which is defined as the average distance travelled by an electron through a material before it is inelastically scattered. The IMFP depends on the kinetic energy of the electron and the nature of the solid. Most elements show very similar IMFP vs. energy relationships see fig 3.7.

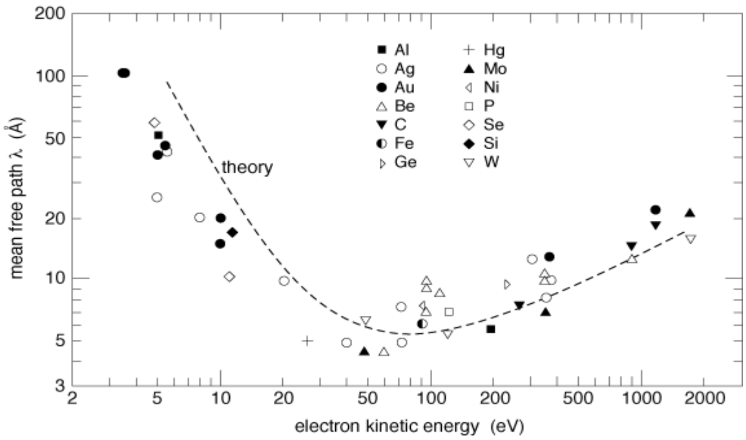

Figure 3.7: compilation of electron mean free path data [61]

As a result of the short mean free path the XPS spectrum contains information only about the top 10 – 100Å of the sample. For determination of the surface composition by x-ray photoelectron spectroscopy, the inelastic mean free path is required for quantitative analyses of homogeneous surfaces [62].

CHAPTER 4

Experimental procedure and data analysis

4.1 ESCA instrument

The (Ga,Mn)As samples were prepared in an MBE (SVTA) system attached to beamline I3 at the synchrotron radiation laboratory MAX-lab. A set of samples were made with different concentrations of Mn in the range 0.5 - 5.5 at %. The nominal concentrations were determined by RHEED oscillations recorded during the growth as described above. The samples were indium-glued on transferrable Mo holders and cleaned by Ar sputtering with ~3keV ions using a current density of ~ 2 μA/cm^2. The instrument used for analysis was an ESCA PHI 5000c system, see Figure 4.1.

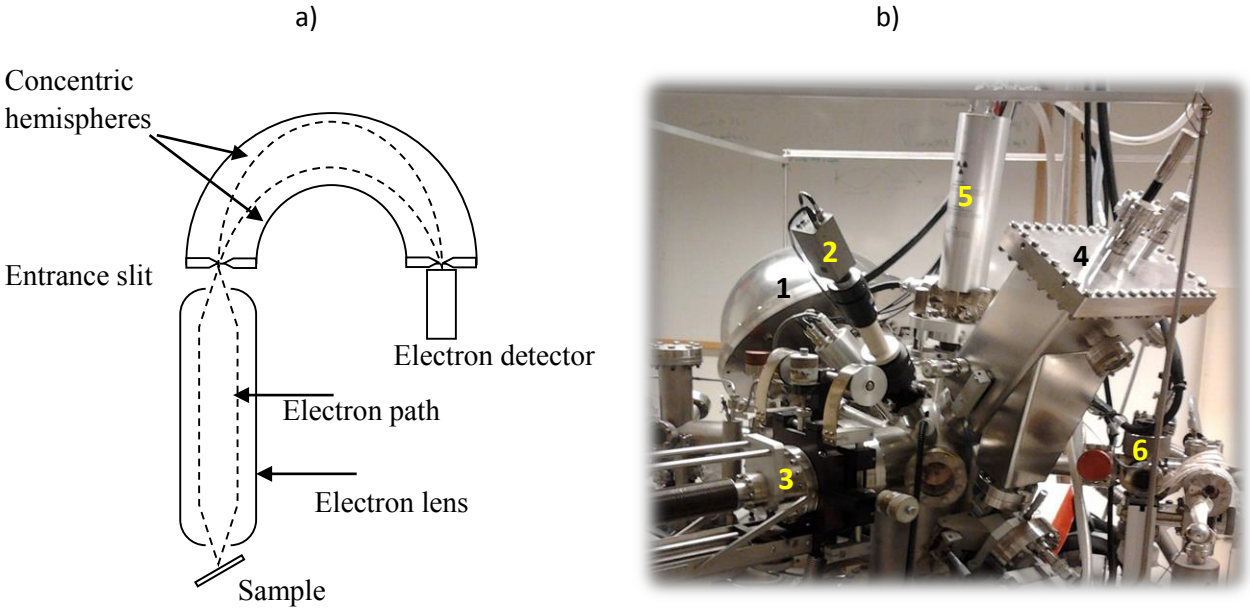

Figure 4.1: a) A schematic diagram of a hemispherical electron energy analyzers. b) ESCA (PHI 5000c) system located at Chalmers Laboratory of Chemical Physics at the department of Applied Physics. The different parts are 1) electron energy analyzer, 2) optical microscope, 3) sample manipulator, 4) monochromatic X-ray source, 5) dual anode X-ray source, 6) sample introduction chamber.

The XPS experiment starts by setting up the sample wafer (~1x1)cm^2 on an XPS sample holder with tweezers to minimize contamination. Then the XPS sample holder is placed into the fast entry air-lock of the introduction chamber. The sample to be measured and the area of interest are then selected using an optical microscope. The XPS spectra were excited with

monochromatised AlK_α radiation (ΔE~0.5eV). Electrons emitted from the sample pass through a lens before getting to the energy analyzer (fig 4.1a). The analyzer consists of concentric metal hemispheres that are at different potentials. Electrons entering the gap between the hemispheres impinge on the outer hemisphere (radius R_2) when they travel too fast and are attracted to the inner hemisphere (radius R_1) when they travel too slow. Only electrons in a narrow energy region around the "pass energy" get all the way between the hemispheres to the detector. As shown in the diagram, the hemispherical analyzer has focusing properties such that electrons entering at different angles converge on the exit slit if they have the pass energy. The pass energy is given by E_p=eKΔV, where the analyzer constant K= $R_1R_2/(R_2^2 - R_1^2)$, e is the charge of the electron and ΔV is the potential difference between the hemispheres. The area probed by the analyzer is ~1mm^2

4.2 Evaluation of concentration

Given an XPS spectrum the concentration C_x of an element X (e.g. Mn) is obtained as

$$C_x = \frac{I_x/S_x}{\sum_i {}^{I_i}/_{S_i}} \quad \dots\dots\dots\dots\dots\dots\dots\dots\dots\dots\dots\dots\dots \ (3)$$

where S_x is the sensitivity factor (including the mean free path λ and photoionization cross section) and I_x is the spectral intensity of element X. The elements included in the evaluation were Ga, Mn and As.

According to equation 3 the error limit of the final result depends on the accuracy of the spectral intensities and on the uncertainty of the sensitivity factors. The factors contributing to the uncertainty in the evaluation of the intensities are the signal statistics (noise) and the correctness of the estimated background. The different types of commonly used backgrounds are the Shirley-Sherwood, Tougaard, polynomial, and exponential functions [64]. Some examples are shown in Fig.4.2.

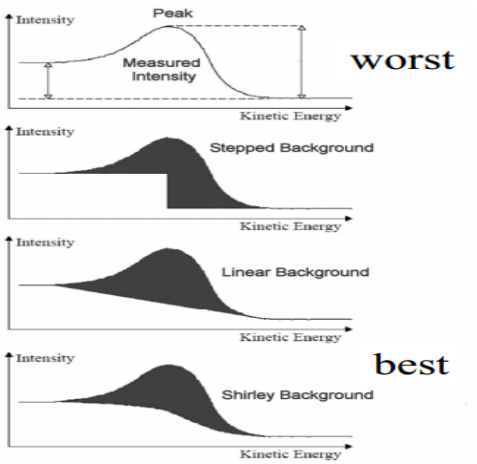

Figure 4.2: Different types of backgrounds[64] in XPS.

To reduce the influence of noise, the quantification of intensities in the present study was based on the integrated peaks, obtained by the following steps:

- Plotting of spectra from each of the elements of (Ga,Mn)As material on an expanded scale (fig.4.3).
- Estimating background function (figs.4.4-4.6).
- Subtracting of the background from the recorded data (fig.4.7).
- Integrating the background free spectrum (fig.4.8).

Due to the low intensity of the Mn signal, and due to its location on a high nonlinear (unknown) background (see Fig.5.1), the choice of background is considered as a main experimental uncertainty factor. The ambiguity is illustrated in Figs. 4.4 – 4.6, which show data fitted with different background functions. Since the simple polynomial function (2^{nd} order) is most similar to the Shirley-Sherwood function result, which (along with the Tougaard backround) is considered to be locally the most correct one, this is the function used in the present evaluations. When estimating the As(3d) and Ga(3d) intensities a linear background was used because of the relatively large heights and narrow widths of the peaks. In these cases the same results were obtained when using other background functions.

Table 4.1: The sensitivity factors for Ga(3d), Mn(2p) and As(3d) found in ref. 63. The values are valid for the standard lens and 90^0 angle between light and electron emission.

Sensitivity factors		
Mn (2p)	Ga (3d)	As (3d)
2.366	0.258	0.446

The sensitivity factor depends on the atomic and crystallographic properties. In addition it also depends on the experimental geometry, specifically the angle between incident light beam and electron emission angle. In the present experiments we have used the tabulated sensitivity factors for the standard lens and 90^0 angle between light and electron directions. In the evaluation of estimated accuracy the uncertainty of the sensitivity factors was thus assumed to be ±0.0005. This is of course a lowest limit of the uncertainty because it does not take into account the fact that our samples are not pure elements but compounds, and that there may be small deviations from the ideal geometrical arrangement. The error limits were evaluated using the extreme results from equation (3):

$$C_{x\,max} = \frac{I_{x\,max}/S_{x\,min}}{\sum_i {I_{i\,min}}/{S_{i\,max}}} \qquad \ldots\ldots\ldots\ldots\ldots\ldots\ldots\ldots\ldots (4)$$

$$C_{x\,min} = \frac{I_{x\,min}/S_{x\,max}}{\sum_i {I_{i\,max}}/{S_{i\,min}}} \qquad \ldots\ldots\ldots\ldots\ldots\ldots\ldots\ldots\ldots (5)$$

$$\Delta C = C_{x\,max} - C_{x\,min}$$

$$C_x = C_{x\,calc} \pm \Delta C$$

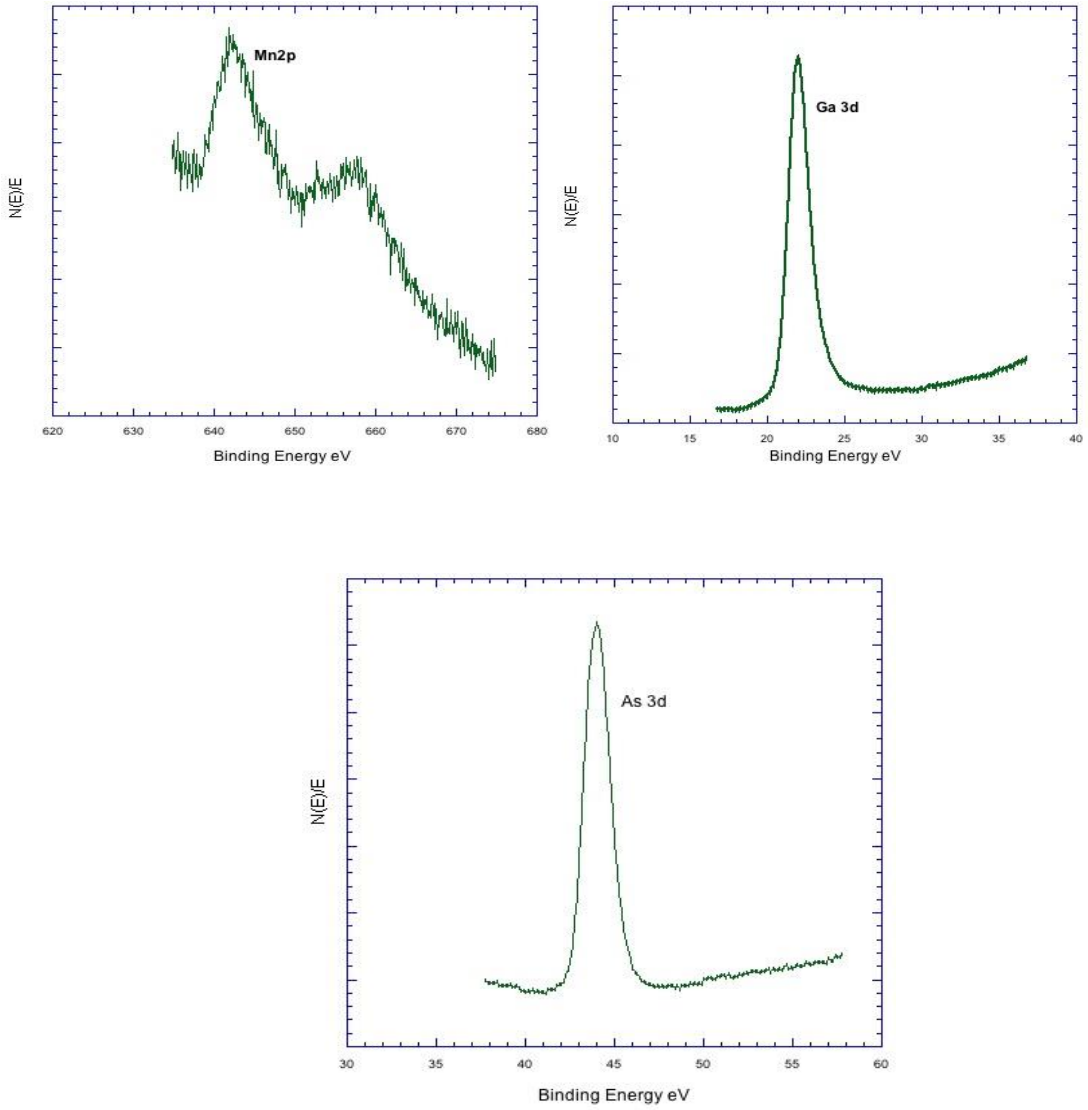

Figure 4.3: Expanded scale plots of Mn, Ga and As spectra

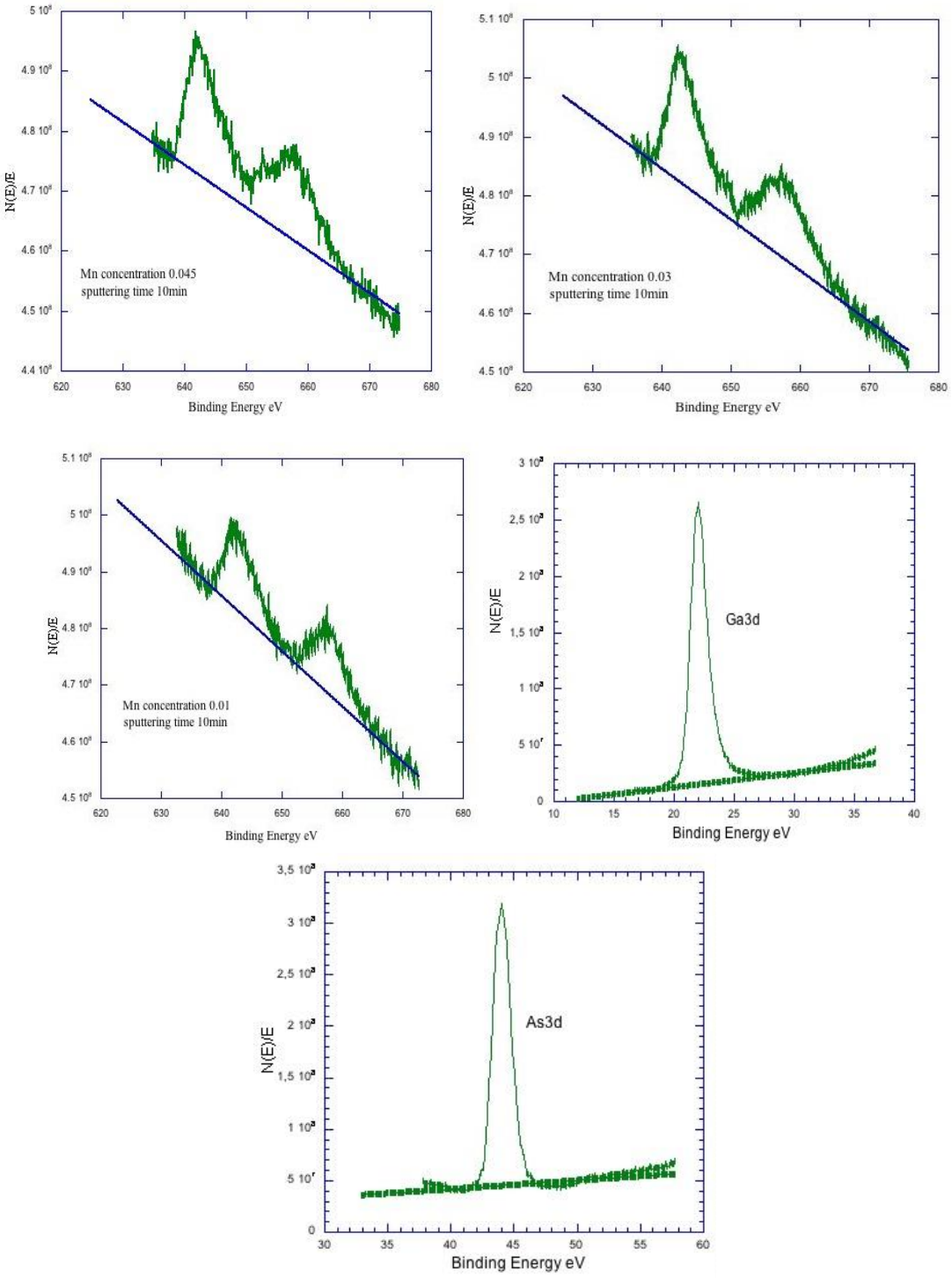

Figure 4.4: Expanded scale Mn2p spectra with linear backgrounds.

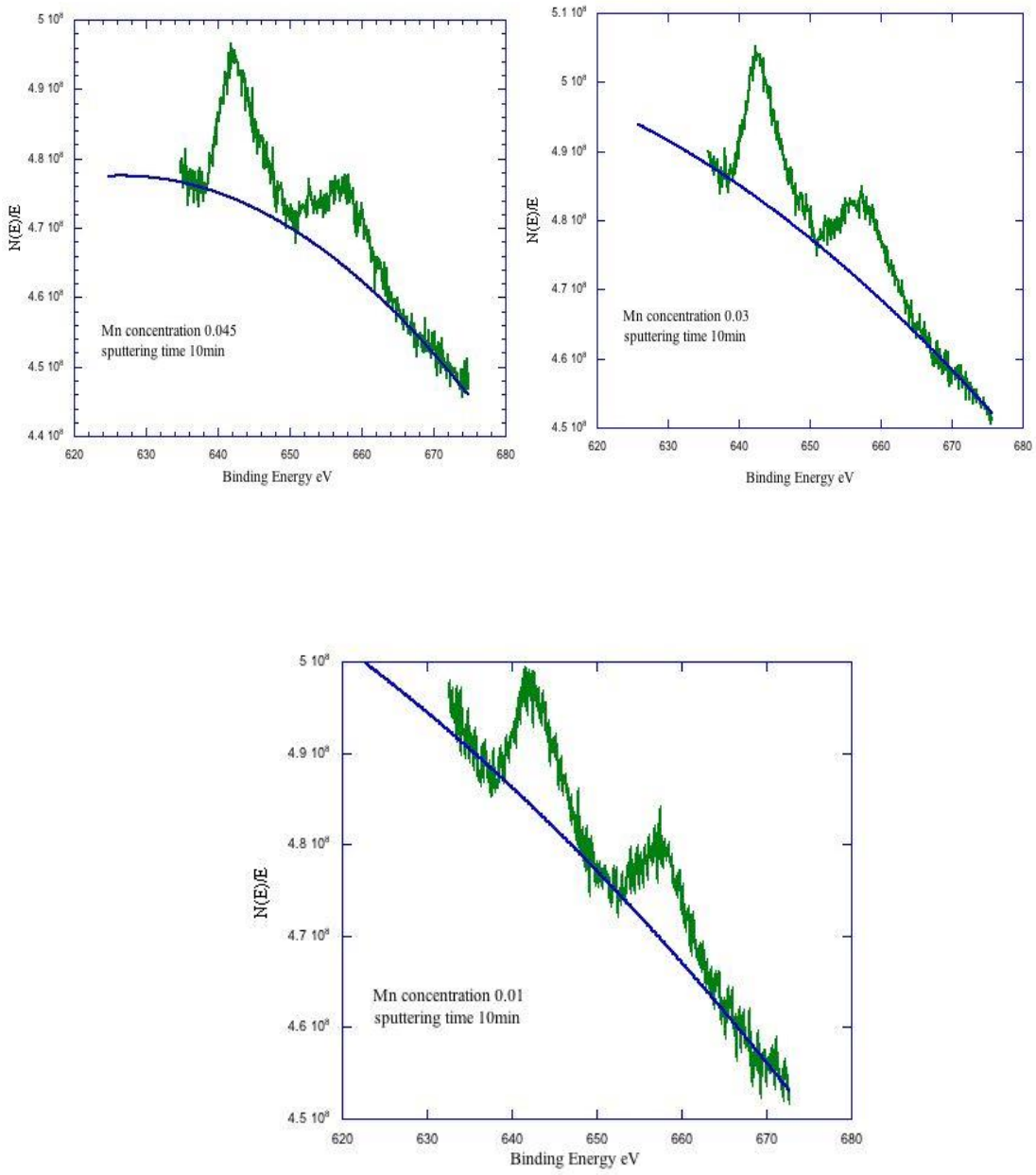

Figure 4.5: Expanded scale Mn2p spectra with polynomial backgrounds

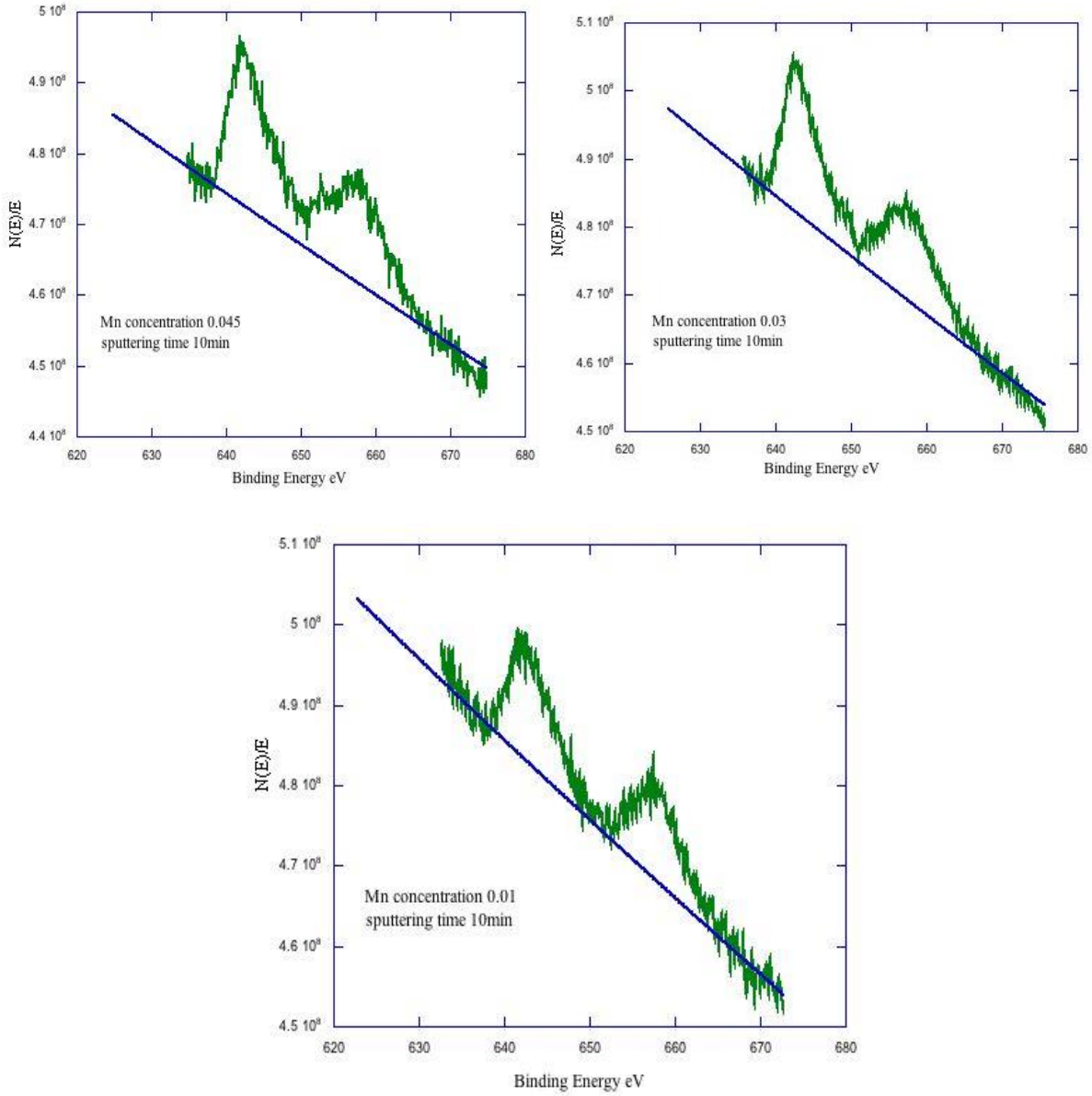

Figure 4.6: Expanded scale Mn2p spectra with exponential backgrounds

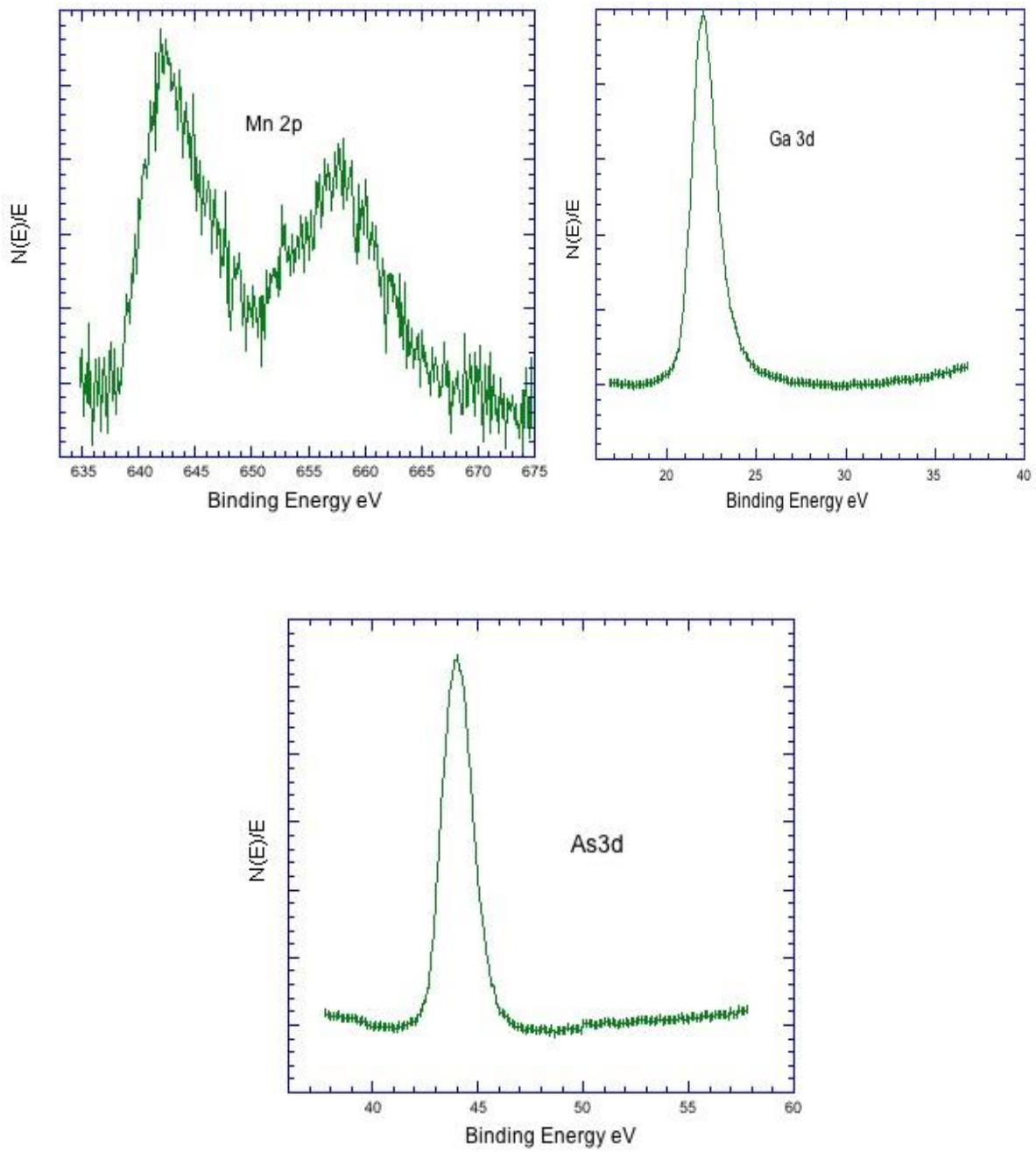

Figure 4.7: Expanded scale Mn2p, Ga3d, and As3d spectra after subtraction from initial backgrounds.

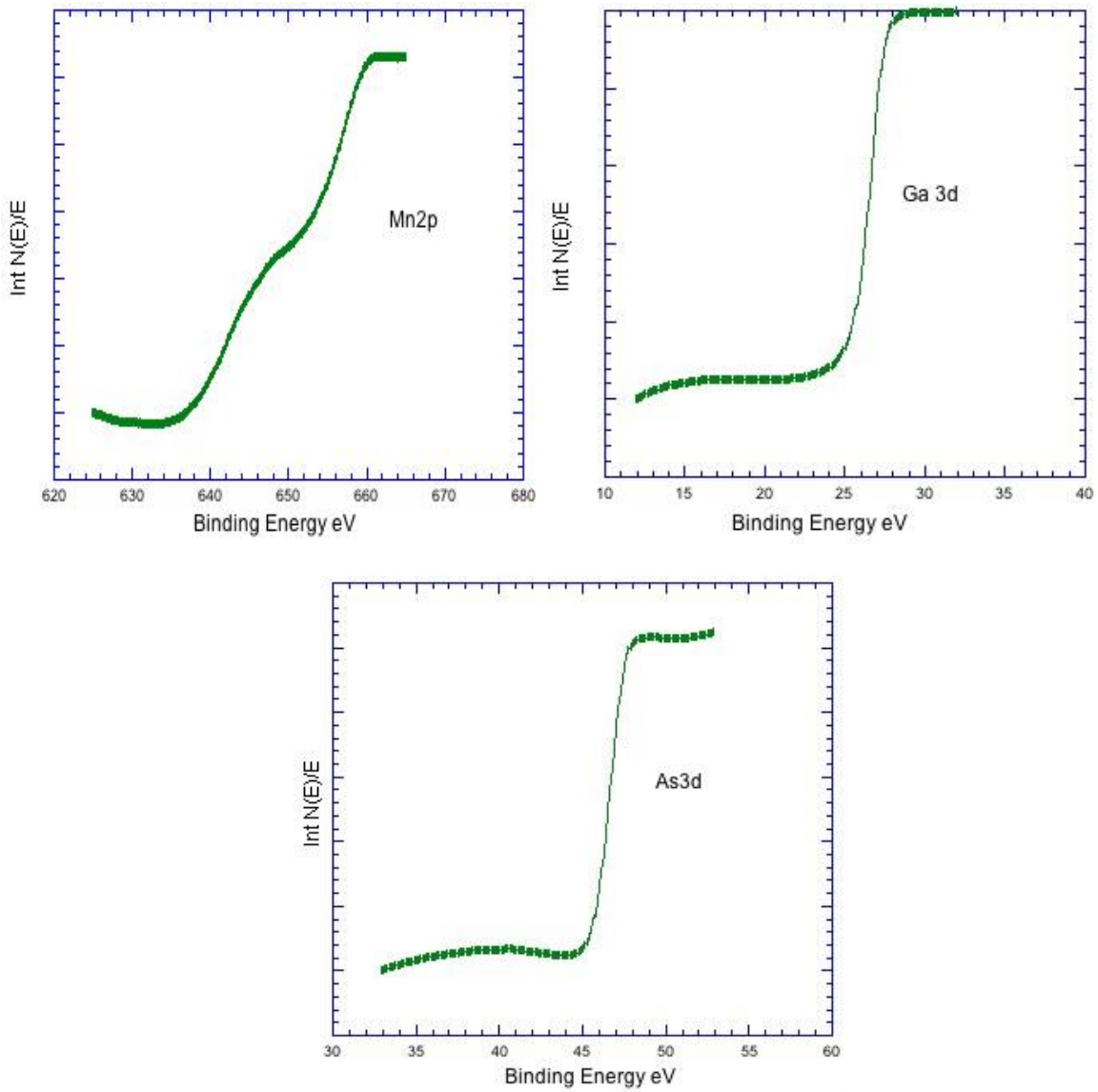

Figure 4.8: Integrated background free Mn2p, Ga3d and As3d spectra.

5 Result and discussion

The first data obtained from each sample is the survey spectrum which covers the full binding energy scale (0-1000 eV), see Fig 5.1. The survey spectra can be used as a reference to follow the degree of surface contamination. From these spectra one can see that before sputtering the Mn signal is very low while there is substantial contamination (oxygen and carbon). As the sample is sputtered the peaks of the Mn 2p can be seen to grow while the oxygen and carbon peaks vanish. The decrease of the survey spectra at binding energies above ~600 eV in Fig 5.1 is caused by the falling lens transmission function as the kinetic energy is reduced.

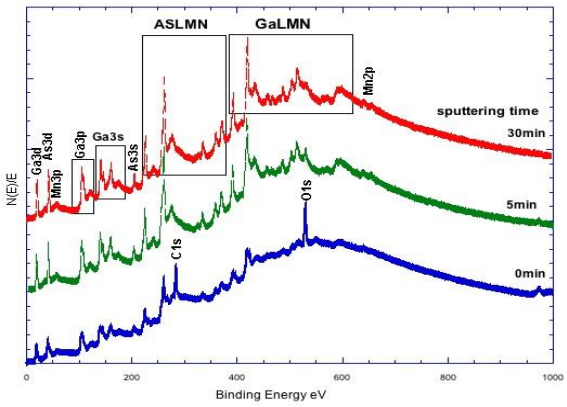

Figure 5.1: Survey spectra for (Ga,Mn)As showing the various peak identification [65]. The graphs have been vertically shifted.

The changes in the Mn signal intensity during sputtering are shown in (Fig 5.2). The Mn concentration after sputtering increases at the beginning of the process because the surface contamination (carbon and oxides) is removed. A maximum intensity is then obtained as a result of out-diffused Mn. At this point the intensity can be as much as 5 times higher than in the bulk [66]. After further sputtering a stable Mn concentration is found, which can be considered to represent bulk concentration.

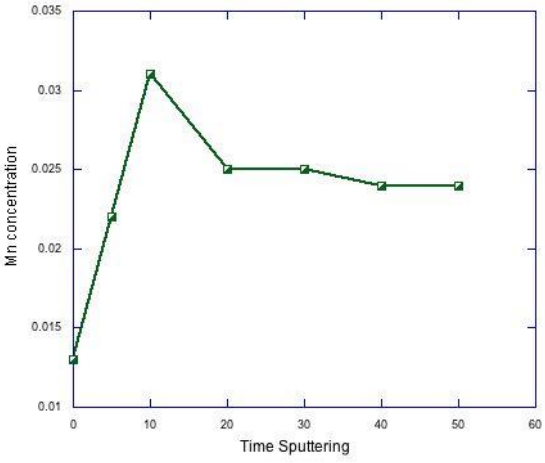

Figure 5.2: Mn signal intensity vs the time of sputtering for the sample with 4.5% nominal concentration.

The results in table 5.1 show the evaluated Mn concentrations for the various samples and the estimated accuracies for each case. The results can be discussed in different ways depending on the mode of measurement i.e. depth profiling or surface mapping. For the sample with the nominal concentration x=0.03 data were recorded at different points, about 2mm apart to look for possible variations in lateral composition. The results indicate indeed different lateral compositions before sputtering. This might be from the non-uniformity of As on the surface. The corresponding As and Ga concentrations at the two points were of 0.37, 0.57 and 0.39, 0.57, which supports this hypothesis.

For the sample with nominal concentration x=0.01 data were recorded at three different points separated by ~ 2mm and then taken back to the first point for further analysis after sputtering. For the sample with nominal concentration x=0.005 the results are shown for measurements at three different surface positions about 2mm apart. To check the reproducibility, two sets of data were recorded after 1min sputtering at the same point. Finally, the sample with x=0.02 was not investigated further because it was cracked.

Since the data set for the sample with 4.5% nominal concentration were most complete, the results on this sample are finally commented in some more detail. The table shows the measurement of the sample surface at the same point but different sputter times and the result was used in plotting the Mn concentration vs. the depth (Fig 5.2). After 40-50 min sputtering the Mn concentration was stabilized at C_{Mn} =0.024±0.006, where the accuracy was obtained according to eq. (4) and (5) with estimated intensity values as shown below:

$I_{Mn\ max}$	$I_{Mn\ min}$	$I_{As\ max}$	$I_{As\ min}$	$I_{Ga\ max}$	$I_{Ga\ min}$
(arb. units)					
181	162	522	449	527	452

The Ga and As concentrations were found to be 0.62 and 0.36, which obviously deviates from the expected values around (0.50 for As and 0.45 for Ga). The reason for the deviating values obtained from the present experiment must be inappropriate sensitivity factors. Clearly, the method depends critically on availability of adequate sensitivity factors.

Table 5.1: overview of Mn concentrations for different samples as function of sputtering times.

Sputter time	**Mn concentration x of $(Ga_{1-x}Mn_x)As$**			
	X=0.045 $Ga_{0.955}Mn_{0.045}As$	X=0.03 $Ga_{0.97}Mn_{0.03}As$	X=0.01 $Ga_{0.99}Mn_{0.01}As$	X=0.005 $Ga_{0.995}Mn_{0.005}As$
0	0.025exp* 0.025lin* **0.013pol***	Point 1 0.054exp 0.054lin **0.055pol**	Point 1 0.036exp 0.035lin **0.025pol**	Point 1 0.032exp 0.032lin **0.016pol**
0		Point 2 0.054exp 0.054lin **0.041pol**	Point 2 0.033exp 0.033lin **0.032pol**	Point 2 0.036exp 0.036lin **0.036pol**
0			Point 3 0.033exp 0.034lin **0.027pol**	Point 3 0.040exp 0.039lin **0.035pol**
1min				Point 1 0.029exp ; 0.030exp 0.028lin ; 0.029lin **0.025pol** ; **0.025pol**
5min	0.029exp 0.029lin **0.022pol**			
7min				0.028exp 0.023lin **0.021pol**
10min	0.039exp 0.039lin **0.031pol**	Point 1 0.033exp ; 0.030exp 0.033lin ; 0.029lin **0.029pol** ; **0.029pol**	0.024exp 0.023lin **0.020pol**	
20min	0.030exp 0.030lin **0.025pol**		0.022exp 0.020lin **0.017pol**	
30min	0.028exp 0.027lin **0.025pol**			
40min	0.022exp 0.022lin **0.024pol**			
50min	0.024exp 0.024lin **0.024pol**			

*exp = exponential background
lin = linear background
pol = polynomial backgroun

Chapter 6

Conclusion

The goal of this project was to test the applicability of XPS for determination of the Mn concentration in (Ga,Mn)As. After removal of a contaminated surface layer it was possible to see a concentration profile caused by out diffusion of Mn. A stable Mn signal vs depth was eventually found. For a sample with a nominal concentration of 4.5% (determined by RHEED oscillations) the present XPS analysis showed a concentration of 2.4±0.6%. The deviation from the nominal value is too large to be considered as correct. A main problem with the XPS method is the limited availability of adequate sensitivity factors. The factors used here were taken from literature and refer to pure elements, while the present evaluation concerns an ordered compound. It is encouraging to see that the precision of the method is quite good even though the accuracy is not. The latter can be improved significantly by using calibrated sensitivity factors obtained from measurement on samples with similar structure and composition as the unknown one.

Reference

1. M. Munekata, Appl. Phys. Lett. 63, 1849 (1989).
2. H. Ohno, Appl. Phys. Lett. 69, 363 (1996).
3. H. Ohno, H. Munekata, T. Penney, S. Von Molnar, L. L. Chang, Phys. Rev. Lett. 68, 2664 (1992).
4. T. Dietl, H. Ohno, F. Matsukura, J. Cibert, and D. Ferrand, Science 287, 1019 (2000).
5. T. Dietl, H. Ohno, and F. Matsukura, Phys. Rev. B 63, 195205 (2001).
6. D. Chiba, K. Takamura, F. Matsukura, and H. Ohno, Appl. Phys. Lett. 82, 3020 (2003).
7. T. Jungwirth, K. Y. Wang, J. MaŠek, K. W. Edmonds, Jürgen König, JairoSinova, M. polini, N. A. Goncharuk, A. H. MacDonald, M. Sawicki, A. W. Rushforth, R. P. Campion, L. X. Zhao, C. T. Foxon, and B. L. Gallagher, Phys. Rev. B 72, 165204 (2005).
8. T. Hayashi, Y. Hashimoto, S. Katsumoto, and Y. Iye, Appl. Phys. Lett. 78, 1691 (2001).
9. K. W. Edmonds, P. Boguslawski, K. Y. Wang, R. P. Campion, S. N. Novikov, N. R. S. Farley, B. L. Gallagher, C. T. Foxon, M. Sawicki, T. Dietl, M. Buongiorno Nardelli, and J. Bernholc, Phys. Rev. Lett. 92, 037201 (2004).
10. J. Sadowski and J. Z. Domagala, Phys. Rev. B69, 75206 (2004).
11. J. Masek, J. Kudrnovsky, and F. Maca, Phys. Rev. B, 67:153203, (2003).
12. M. Tanaka, J. Vac. Sci. Technol. A 18, 1247 (2000).
13. M. Tanaka, J. Vac.sci. Technol. B 16, 2267 (1998).
14. M. Sawicki, Phys. Rev. B 70, 245325 (2004).
15. H. X. Tang, R. K. Kawakami, D. D. Awschalom and M. L. Roukes, Phys. Rev. Lett. 90, 107201, 2003.
16. X. Liu, Y. Sasaki, and J. K. Furdyna, Phys. Rev. B 67, 205204,2003.
17. T. Lungwirth, I. Sinova, I. Masek, I. Kucera, and A. H. MacDonald, Rev. Mod. Phys. 78, 809-864 (2006).
18. O. Yastrubchak, J. Sadowski, H. Krzyżanowska, L. Gluba, J. Żuk, J.Z Domagala, T. Andrearczyk, T. Wosinski. Journal of Applied Physics 114, 053710, 2013.
19. J. Schneider, U. Kaufmann, W. Wilkening, and M. Baeumler, Phys. Rev. Lett. 59, 240-243(1989).
20. "New semiconductor materials. Characteristics and properties" http://www.ioffe.rssi.ru/SVA/NSM/Semicond/GaAs/bandstr.html. [online; accessed 2013-11-10]
21. I. R. Arthur, Ir., J. Appl. Phys., 39:4032 (1968).

22. A. Y. Cho, J. Vac. Sci. Technol., 8:S31 (1970).
23. N. C. Cirillo Jr, M. S. Shur, and J. K. Abrokwah., Elec. Dev. Lett., EDL-7 71 (1986).
24. K. Kamei, H. Kawasaki, S. Hori, K. Shibata, M. Higashiura, M.O. Watanabe, and Y. Ashizava, 12th Int'l. Symp. GaAs and Related Compounds, Karuizawa, Jpn., 1985, Inst. Phys. Conf. Ser., 79:541 (1986).
25. G.J. Sullivan, P. M. Asbeck, M.F. Chang, D.L. Miller, and K.C. Wang, Electron. Lett., 22:419 (1986).
26. T. I. Drummond, W. Koop, D. Arnold, R. Fischer, H. Morkoc, L.P. Erickson, and P. W. Palmberg, Electronic Lett., 19:986 (1983).
27. G.W. Taylor, J.G. Simmons, R.S. Mand, and A.Y. Cho, J. Vac. Sci. Technol. B, 4:603 (1986).
28. J. Xu, and M. Shur, IEEE Electron Device Letters, EDL-7:416 (1986).
29. A. Y. Cho, C. N. Dunn, R. L. Kuvas, and W.E. Schroeder, Appl Phys. Lett., 25:224 (1974).
30. T. L. Hierl, and P. E. Luscher, Proc. 2nd Int'l. Symp. on MBE and Clean Surface Techniques, p. 147, Tokyo, Jpn. (1982).
31. H. D. Shih, and B. Bayraktaroglu, J. Vac. Sci. Technol., B2:269 (1984).
32. R. A. Linke, M.V. Schnieder, and A. Y. Cho, IEEE Trans. on Microwave Theory and Tech., MTT-26:935 (1978).
33. J. J. Harris, and J .M. Woodcock, Electron. Lett., 16:317 (1980).
34. J. P. Nagle, L. A. Hing, T. M. Kerr, and J. G. Summers, J. Vac. Sci. Technol., B4:631 (1986).
35. W. H. Haydl, R. S. Smith, and R. Bosch, Appl. Phys. Lett., 37:556 (1980).
36. A. Y. Cho, and F. K. Reinhart, J. Appl. Phys., 45:1812 (1974).
37. S. Katsumoto, A. Yamamoto and M. Yamaguchi, Jpn. J. Appl. Phys., 24:636 (1985).
38. D. A. B. Miller, The 2nd Int'l. Conf. on Modulated Semi. Structures, Collected Papers, p. 459, Kyoto, Jpn. (1985).
39. T. P. Pearsall, H. Temkin, J. C. Bean and S. Luryi, Elec. Dev. Lett., EDL- 7:330 (1986).
40. H. Q. Tserng, and B. Kim, IEEE GaAs IC Symposium, p. 11, Monterey, CA (1985).
41. K. C. Wang, P. M. Asbeck, M. F. Chang, D. L. Miller and F. H. Eisen, IEEE GaAs IC Symp., p. 99, Monterey, CA (1985).
42. N. Kobayashi, S. Notomi, M. Suzuki, T. Tsuchiya, K. Nishiuchi, K. Odani, A. Shidatomi, T. Mimura, and M. Abe, IEEE GaAs IC Symp., p. 207, Monterey, CA (1985).

43. S. Kuroda, I. Mimura, M. Suzuki, N. Kobayashi, K. Nishiuchi, A. Shibatomi, and M. Abe, IEEE AsAsIC Symp., p. 133, Monterey, CA (1984).
44. W. D. Goodhue, B.E. Burke, K.B. Nichols, G. M. Metze and G.D. Johnson, J. Vac. Sci Technol., B4:769 (1986).
45. P. M. Asbeck, D. L. Miller, R.J. Anderson, R. N. Deming, R. T. Chen, C. A. Liechti, and F. H. Eisen, IEEE GaAs IC Symp., p. 133 (1984).
46. O. Wada, I. Sanada, H. Hamaguchi, T. Fujii, S. Hiyamizu, and I. Sakurai, Jpn. J. Appl. Phys., 22(22-1):587 (1983).
47. J. Barnard, H. Ohno, C. E. C. Wood, and L.F. Eastman, IEEE Elect. Dev. Lett., EDL-2:7 (1981).
48. E. Wake, E. G Scott, and I. D Henning, Electron. Lett., 22:719 (1986).
49. H. Wang and D. Ankri, Electron. Lett., 22:391 (1986).
50. H. Matsueda, M. Hirao, T. Tanaka, H. Kodera, and M. Nakamura, Int'l. Symp. GaAs and Related Compounds, Karuizawa, Jpn., (1985); Inst. Phys. Conf. Ser., 79:655 (1986).
51. T. Fujii, S. Yamakoshi, K. Nanbu, O. Wada, and S. Hiyamizu, J. Vac.Sci.Technol.B2:259 (1984).
52. R. D Burnham, and D. R Scifres, Integrated Optical Devices Fabricated by MBE, in: Prog. Crystal Growth Charact., 2:95 (1979); and E.M Conwell, and R.D Burnham, Materials for Integrated Optics: GaAs, Ann. Rev. Mater. Sci., 8:135 (1978).
53. S. Sakano, H. Inoue, H. Nakamura, T. Katsuyama, and H. Matsumura, Electron. Lett., 22:594 (1986).
54. F. K Reinhart and A. Y. Cho, Appl. Phys. Lett., 31:457 (1977).
55. H. Ishikawa, N. Takagi, S. Ohsaka, K. Hanamitsu, T. Fujiwara, and M. Takusagawa, Appl. Phys. Lett., 36:520 (1980).
56. G. Biasiol and L. Sorba, “Molecular beam epitaxy: principles and applications”, in Crystal growth of materials for energy production and energy-saving applications, R. Fornari, L. Sorba, Eds. pp. 66-83(Edizioni ETS, Pisa, 2001).
57. J. Sadowski, GaMnAs: Layers, Wires and Dots, 2008.
58. J. H. Neave, B. A. Joyce, P. J. Dobson and N. Norton, Appl. Phys. A 31(1):1, 1983.
59. C. Nordling, E. Sokolowski, K. Siegbahn, Phys. Rev. 105, 1676 (1957).
60. J. C. Vickerman and S. Gilmore, Surface Analysis- The principal Techniques, 2nd Edition, 2009.
61. A. Zangwill, Physics at the surfaces, cambridge univ. press, cambridge (1988).
62. A. Jablonski, C.J. Powell, surf. Interface Anal. 20, 771(1993).

63. C. D. Wagner, L. E. Davis, M. V. Zeller, J. A. Taylor, R. M. Raymond and L. H. Gale, Surf. Interface Anal., 3. 211 (1981).
64. Tougaard and Sigmund, Phys. Rev. B 25, 4452 (1982).
65. C. D. Wagner, W. M. Riggs, L. E. Davis, J. F. Moulder. Handbook of X-ray Photoelectron Spectroscopy. Perkin –Elmer Corporation, Physical Electronics Division, 1978.
66. M. Adell, J. Adell, L. Ilver, J. Kanski and J. Sadowski, Appl. Phys. Lett. 89, 172509 (2006).